Applied Physics Letters

Photoconductivity effect in SnTe quantum well

Cite as: Appl. Phys. Lett. **119**, 032104 (2021); https://doi.org/10.1063/5.0056230
Submitted: 07 May 2021 . Accepted: 13 July 2021 . Published Online: 22 July 2021

G. R. F. Lopes, S. de Castro, B. Kawata, P. H. de O. Rappl, E. Abramof, and M. L. Peres

ARTICLES YOU MAY BE INTERESTED IN

Universal alignment of surface and bulk oxygen levels in semiconductors
Applied Physics Letters **119**, 021601 (2021); https://doi.org/10.1063/5.0052521

Temperature dependence of the picosecond spin Seebeck effect
Applied Physics Letters **119**, 032401 (2021); https://doi.org/10.1063/5.0050205

Comparison and analysis of $Al_{0.7}InAsSb$ avalanche photodiodes with different background doping polarities
Applied Physics Letters **119**, 032101 (2021); https://doi.org/10.1063/5.0056300

QBLOX
Shorten Setup Time
Auto-Calibration
More Qubits

1 qubit
Fully-integrated
Quantum Control Stacks
Ultrastable DC to 18.5 GHz
Synchronized <<1 ns
Ultralow noise

100s qubits
visit our website >

© 2021 Author(s).

Photoconductivity effect in SnTe quantum well

Cite as: Appl. Phys. Lett. **119**, 032104 (2021); doi: 10.1063/5.0056230
Submitted: 7 May 2021 · Accepted: 13 July 2021 ·
Published Online: 22 July 2021

G. R. F. Lopes,[1] S. de Castro,[2,a)] B. Kawata,[3] P. H. de O. Rappl,[3] E. Abramof,[3] and M. L. Peres[1]

AFFILIATIONS

[1]Instituto de Física e Química, Universidade Federal de Itajubá, Itajubá, CEP 37500-903 Minas Gerais, Brazil
[2]Universidade do Estado de Minas Gerais, Divinópolis, CEP 35501-170 Minas Gerais, Brazil
[3]Laboratório Associado de Sensores e Materiais, Instituto Nacional de Pesquisas Espaciais, São José dos Campos, CEP 12201-970 São Paulo, Brazil

[a)]Author to whom correspondence should be addressed: marcelos@unifei.edu.br

ABSTRACT

We investigated the photoconductivity effect observed in a *p*-type SnTe quantum well in the temperature range of 1.9–100 K. The negative photoconductivity effect is observed for temperatures below 4 K, and it is strongly dependent on the light wavelength. A systematic analysis of the photoconductivity indicates that the origin of the negative photoconductivity is not related to the topological surface states but rather to the reduction of carrier mobility when the SnTe quantum well is illuminated with energies above 2 eV.

Published under an exclusive license by AIP Publishing. https://doi.org/10.1063/5.0056230

The phenomenon of photoconductivity provides an important tool for the investigation of carrier dynamics and its interactions with the band structure of a material. The observation of effects such as negative photoconductivity (NPC), in which the material undergoes a drop in the conductivity in the presence of light, and persistent photoconductivity (PPC), in which the conductivity takes a longer time to return to its initial value after illumination is removed, constitute a set of tools that enables the quantitative determination of the mechanisms responsible for the dynamics of carriers, e.g., helping to locate defect states and to calculate trap ionization energy. These effects have been widely explored in different materials such as Cu_2Se photodetectors,[1] Cd_3As_2 nanowires,[2] Cs_4PbBr_6 single crystals,[3] Ga_2O_3 photodetectors,[4] and carbon nanotubes networks.[5]

Regarding the photoconductivity effect for IV–VI compounds, a more detailed analysis is found in the literature for lead-based compounds such as the pseudo-binaries $Pb_{1-x}Eu_xTe$ and $Pb_{1-x}Sn_xTe$.[6–8] Tavares *et al.*[6] showed that for the alloy $Pb_{1-x}Sn_xTe$, with $x \sim 0.44$, the NPC effect is present even at room temperature. This behavior is associated with defect states that alter the carrier dynamics via generation and recombination rates when the sample is under illumination. In this case, a competition between the generation and recombination mechanisms is observed as a function of temperature and a level of disorder of the system, introduced by the Sn atoms. On the other hand, both the NPC and PPC effects are observed in a *p*-type $Pb_{1-x}Eu_xTe$ film,[7,8] where these phenomena are also related to the presence of defect states in the bandgap, which alters the generation and recombination rates and becomes more evident at lower temperatures since trapping is more effective as temperature decreases.

The narrow gap semiconductor SnTe is a binary compound that possesses promising physical properties with potential application for the development of optoelectronic devices, broadband photovoltaic detectors,[9] thermoelectric devices,[10,11] solar cells,[12] and photodetectors.[13] A few years ago, SnTe was identified as a topological crystalline insulator (TCI), where the metallic surface states are protected by crystal symmetries thanks to the rock salt structure of this compound.[14] Due to the TCI phase, quantum coherent transport was observed in SnTe thin films,[15] as well as other quantum effects such as Shubnikov–de Haas oscillations and weak-antilocalization.[16,17] It also presents a positive photoconductivity effect, investigated in a SnTe:Si film.[13]

In this paper, we present a detailed study of the electrical transport properties and the photoconductivity effect in a 30 nm-wide SnTe quantum well (QW). It was observed that the QW was sensitive to broadband light, ranging from infrared (IR) to ultraviolet (UV) light in a wide range of temperatures. Also, it was observed a transition from positive to negative photoconductivity as temperature is reduced below 4 K, when the sample is illuminated with energies above 2 eV. We show that a simple classical model is able to explain the transition from positive photoconductivity to negative photoconductivity considering the variations of carrier concentration and carrier mobility when the sample is under illumination. We show that the reduction of carrier mobility leads to the NPC effect. We also found that there is no indication of contribution from topological surface states to the electric transport and photoconductivity in the SnTe QW.

The *p*-type SnTe quantum well was grown by molecular beam epitaxy (MBE), using a Riber 32P system, on (111) BaF_2

Published under an exclusive license by AIP Publishing

monocrystal substrates. The sample structure is a 30 nm-wide SnTe layer embedded with a 1.5 μm $Pb_{0.9}Eu_{0.1}Te$ buffer and a 300 nm $Pb_{0.9}Eu_{0.1}Te$ cap layer. The Eu content $x \sim 0.10$ provides the quantum confinement since barriers are completely insulators for this Eu concentration.[18] The electric contact preparation follows the van de Pauw geometry [see the inset in Fig. 1(a)] using gold wires soldered with indium pellets. The indium diffuses through the heterostructure and crosses the layers (barriers and the well). The electric measurements were carried out using a physical property measurement system (PPMS) from Quantum Design composed of a He-cooled superconducting system with the magnetic field up to 9 T and an operating temperature of 1.9–400 K. The optical excitation was provided by light-emitting diodes (LEDs) with wavelengths $\lambda = 398$, 449, 568, 591, 634, and 940 nm and a constant excitation current of 7 mA.

Figure 1(a) shows the metallic behavior of R(T) under dark and light (UV LED) conditions indicating that the transport occurs in the QW in both situations. The schematic illustration of the fabricated contacts and the LED position is an inset of Fig. 1(a). The Ohmic contacts were tested before the photoconductivity measurements. Figure 1(b) shows the I–V curves of the sample measured at 300, 100, and 4.2 K, and the linear dependences indicate that contacts are Ohmic. Figure 1(c) represents the sample structure, indicating the substrate, the buffer, the QW, the cap layer, and the applied magnetic field in the (111) direction, which will be used to further discussion later in the text.

Figure 2(a) presents the time dependence of normalized photoconductivity σ/σ_0, where σ_0 is the conductivity in the dark conditions, for temperatures ranging from 1.9 to 100 K, when the sample is illuminated by IR light. All the curves present the positive photoconductivity effect in the whole range of temperatures, i.e., conductivity increases under illumination and $\sigma/\sigma_0 > 1$. The illumination is switched on and off in the positions indicated by the arrows in this figure. In addition, a strong PPC effect is observed for lower temperatures. The maximum amplitude of the photoconductivity, σ_M, increases as the temperature decreases down to 10 K, but starts to decrease below this temperature, as observed in Fig. 2(c). This behavior reveals the presence of trap levels that are active in this temperature region and are also responsible for the persistent effect.[19] Figure 2(b) shows the values of σ/σ_0 as a function of time when the sample is illuminated by UV light. Similar to the case when the sample is illuminated with IR light, the maximum amplitude increases as the temperature decreases from 100 to 10 K. However, a transition from positive to NPC takes place for lower temperatures. This effect is more clear in Fig. 2(d), where around 3.9 K σ/σ_0 becomes smaller than 1 (see arrow). The drastic variation of the σ_M is observed and may also be related to trapping levels.

Information about trap levels can be obtained from the analysis of decay curves of the photoconductivity once they follow the relation $\sigma = \sigma_0 \exp\left(-\frac{t}{\tau}\right)$, where τ is the recombination time. For this sample, the decay curves are well fitted for the whole temperature range if we consider a combination of two exponentials $\sigma = \sigma_{01}\exp(-\frac{t}{\tau_1}) + \sigma_{02}\exp(-\frac{t}{\tau_2})$, suggesting the presence of two trap levels.[20] The fittings using this combination are presented in the inset of Figs. 3(a) and 3(b) at 75 K. From the fittings, two recombination times are extracted, one shorter (τ_1), that can be from shallower traps, and one longer (τ_2), due to deeper traps. The activation energy $\Delta\varepsilon$ of the trap level, i.e., the barrier energy that carriers have to overcome to recombine, can be obtained using the expression $\tau = \tau_0\exp(-\frac{\Delta\varepsilon}{k_B T})$. Figures 3(a) and 3(b) show the natural logarithm plots of τ as a function of $1/k_B T$ when the sample is illuminated with IR and UV light, respectively. In Fig. 3(a), two regions can be observed and the trap energies obtained are $\Delta\varepsilon_1 \sim (0.24 \pm 0.02)$ meV, at lower temperatures, and

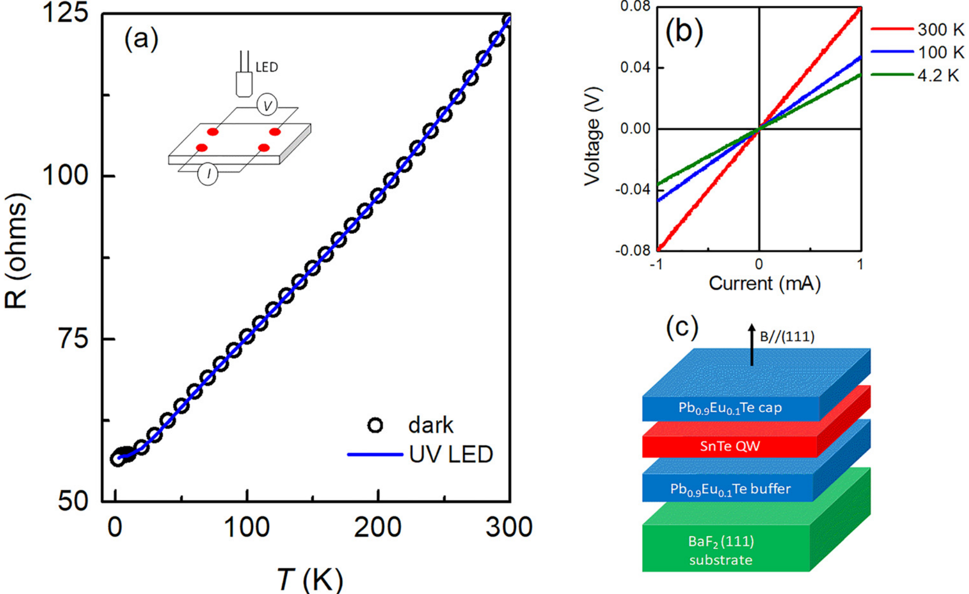

FIG. 1. (a) Electrical resistance as a function of temperature showing metallic behavior indicating that the transport occurs in the well, the inset shows the schematic of the contacts of the sample. (b) I–V curves for Ohmic contacts of the SnTe QW at 300, 100, and 4.2 K. (c) Structure of the quantum well and the applied magnetic field along the (111) direction.

Published under an exclusive license by AIP Publishing

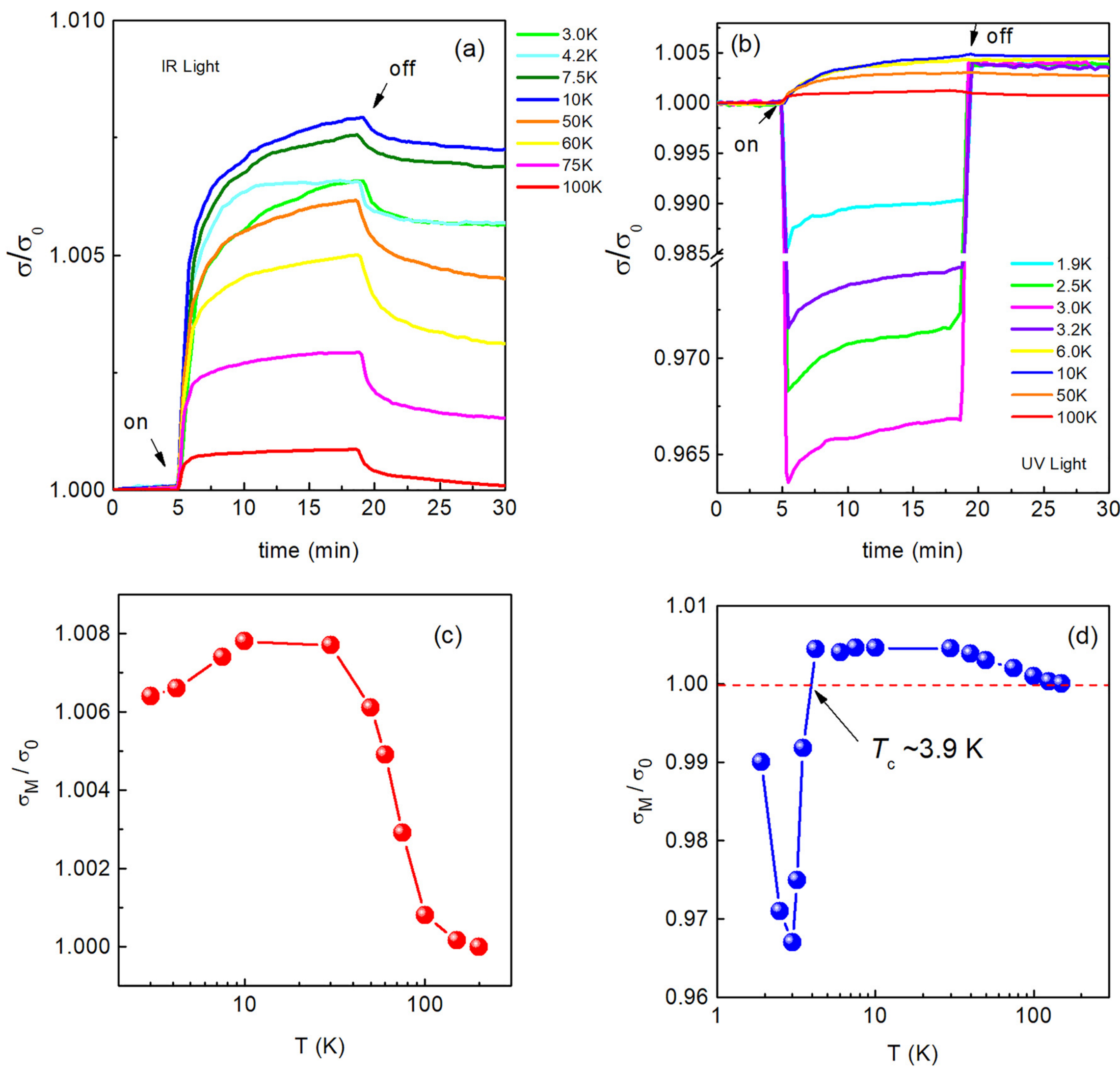

FIG. 2. Time dependence of the normalized photoconductivity in the SnTe QW in the temperature range of 1.9–100 K under IR radiation in (a) and UV irradiation in (b). The arrows indicate the moment of switching on and off illumination. (c) Maximum amplitude of the photoconductivity normalized due to IR, and (d) UV illumination as a function of temperature.

$\Delta\varepsilon_2 \sim (7.1 \pm 0.8)$ meV at higher temperatures. The temperatures for which the thermal energy k_BT corresponds to the trapping levels $\Delta\varepsilon_1$ and $\Delta\varepsilon_2$ are $T \sim 2.8$ and 81.2 K, respectively, i.e., above these temperatures the trapping mechanism becomes less effective.

For the case when the sample was illuminated by UV light, we found $\Delta\varepsilon_3 \sim (32 \pm 6)$ meV, see Fig. 3(b). The temperature for which thermal energy corresponds to 32 meV is $T \sim 371$ K. This temperature is much higher than the temperature for which the photoconductivity effect was observed in the SnTe QW [see Fig. 2(b)] when light is switched off, which explains well why the sample presents the high persistent effect after being illuminated by the UV LED. Figure 3(c) displays the time-dependent photoconductivity curves for UV and IR light at 100 K. In fact, even at 100 K, one can observe that the sample exhibits a strong persistent effect after being illuminated by UV light when compared to the situation where the sample is illuminated with IR light. This indicates that $\Delta\varepsilon_3$ is located inside the band above 2 eV in L point for the SnTe band structure since this trap level is accessed only when the sample is illuminated by UV light with ~3.4 eV. This observation is further corroborated by the fact that when the sample was illuminated by IR light, $\Delta\varepsilon_3$ is not observed. Figure 3(d) shows a schematic representation of the QW structure, where the wider gaps correspond to the barriers, and the narrow gap corresponds to SnTe. In the region of the QW, the valence and conduction bands are inverted (see inverted colors), representing the band inversion caused by the strong spin–orbit coupling in this compound. Under IR illumination, carriers are photogenerated from the valence band to the conduction band (process 1), which causes the positive photoconductivity. The photogenerated carrier remains in the conduction band and, after

Published under an exclusive license by AIP Publishing

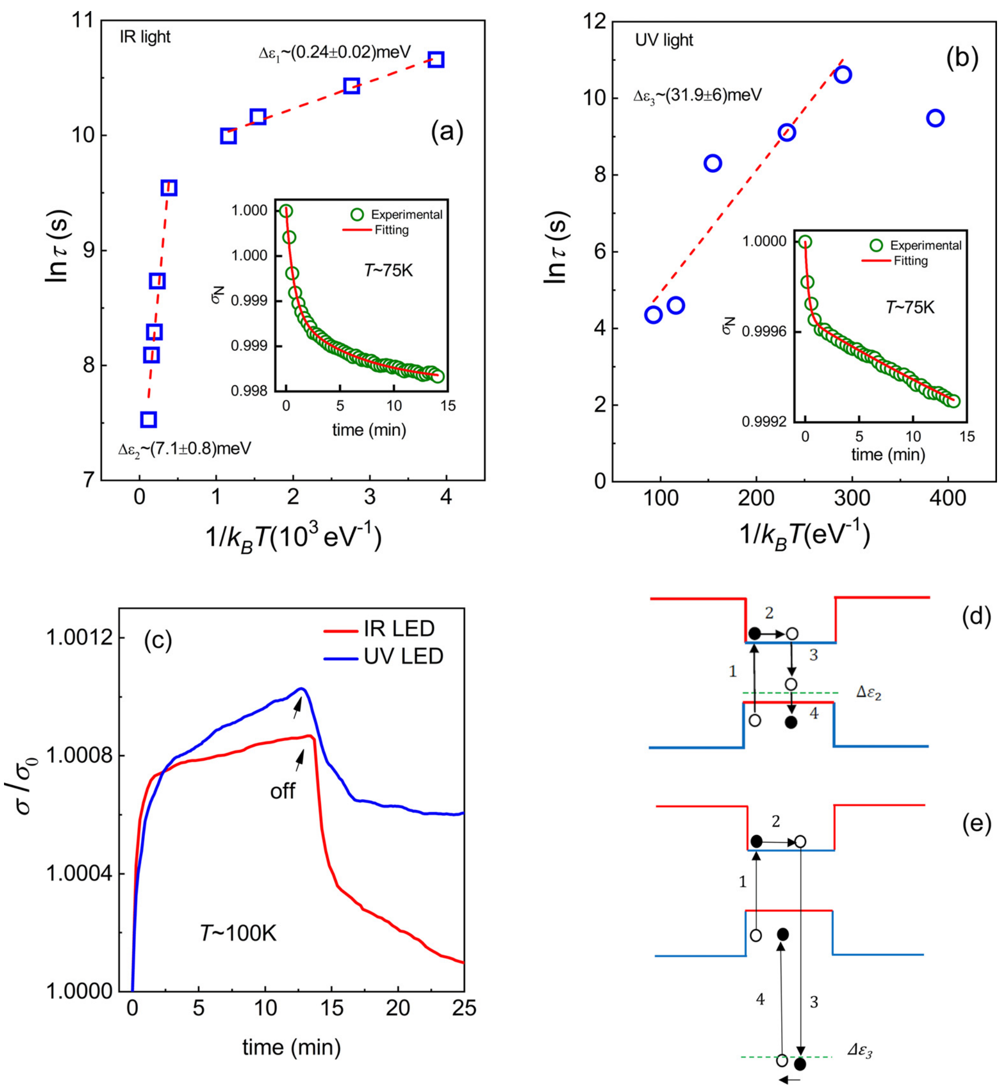

FIG. 3. Arrhenius plot for the SnTe QW. The relaxation time τ was obtained from decay curves after switched off the (a) IR and (b) UV LED. The dashed lines represent a fitting using two exponentials. The insets show the photoconductivity decay at 75 K together with the fitting using two exponentials. (c) The photocurrent measurement as a function of time in the presence of UV and IR light at 100 K. Pictorial representation of the quantum well illuminated by (d) IR and (e) UV lights. The colors show the inversion of the conduction and valence bands in the well. Open and dark circles represent the holes and electrons, respectively.

a given time, it recombines in the defect level with energy barrier $\Delta\varepsilon_2$ (processes 2 and 3). The trapping in this level causes the persistent effect and, after a certain time, the carrier recombines back in the valence band (process 4). Figure 3(e) represents the QW structure illuminated by UV light. Under illumination, the electrons are photogenerated from the valence band to the conduction band, where they remain from a certain time (processes 1 and 2). After that, electrons decay to the defect level with energy barrier $\Delta\varepsilon_3$ (process 3) leading to the persistent effect when the sample is under UV light illumination. Later, electrons recombine back to the valence band (process 4).

To quantitatively investigate the origin of the NPC effect observed under UV light, as shown in Fig. 2(b), Hall measurements were performed on the SnTe QW structure in the range of 1.9–300 K, under UV illumination (on) and dark conditions (off). Figure 4(a) shows the carrier concentration as a function of temperature. In dark conditions, one observes that the carrier concentration increases as temperature decreases and reaches a maximum value around 100 K and then drops slightly as temperature is lowered. For temperatures below ~100 K, carriers cease to be thermally promoted to the valence band and are trapped in the level instead, which causes the decrease in the hole concentration observed. In fact, 100 K corresponds to the thermal energy (k_BT) of 8.6 meV, which is close to the value of the trap level $\Delta\varepsilon_2 \sim (7.1 \pm 0.8)$ meV obtained from the photoconductivity results presented earlier. However, when the sample is under illumination by the UV LED (open squares), an increase in the hole concentration is observed below 100 K due to the photogenerated

Published under an exclusive license by AIP Publishing

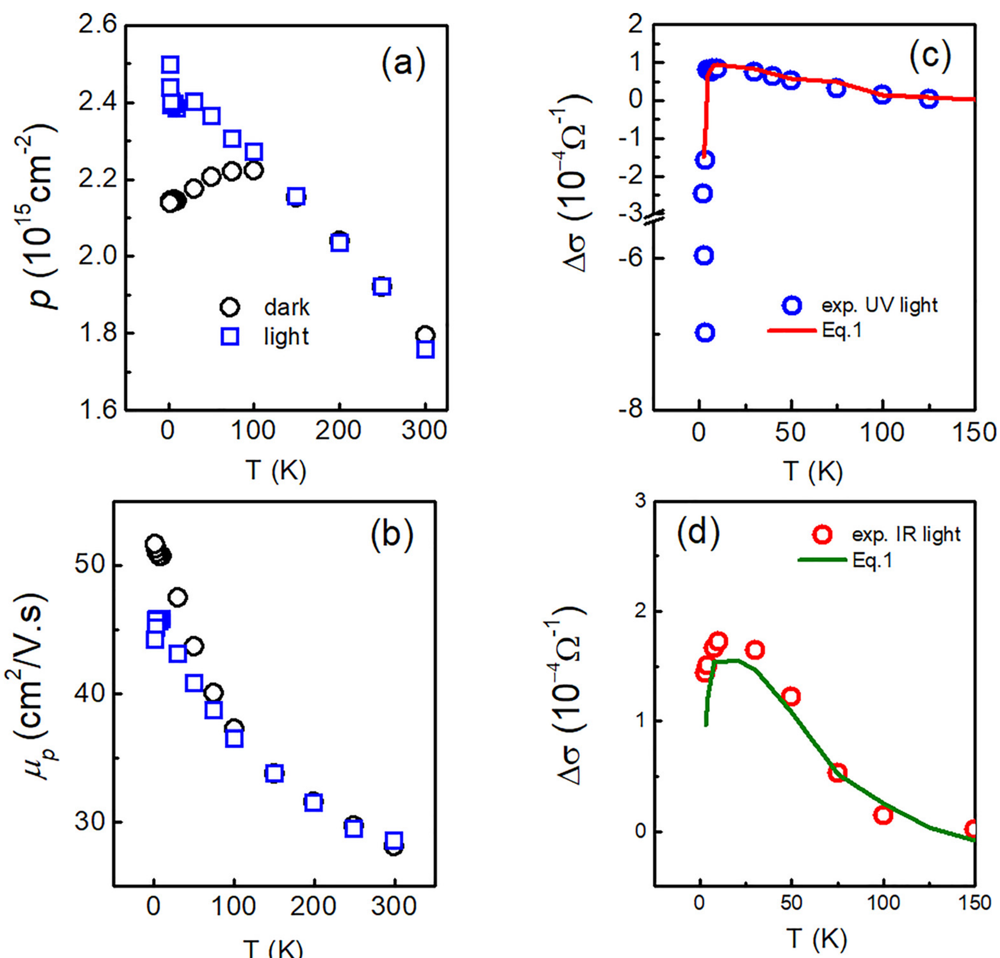

FIG. 4. (a) Hole concentration and (b) Hall mobility in dark conditions (open circles) and under illumination by a UV LED (open squares) of the SnTe QW measured as a function of temperature. (c) and (d) show the comparison between experimental and theoretical values of $\Delta\sigma$ as a function of temperature when the sample is illuminated by the UV LED and the IR LED, respectively.

carriers from traps and from the valence band to the conduction band. For $T > 100$ K, the photogenerated carriers are negligible due to the high recombination rate and do not contribute to the total carrier concentration. Figure 4(b) presents the carrier mobility as a function of temperature under light and dark conditions. Without illumination, a decrease in temperature leads to an increase in carrier mobility as expected. Under illumination, the behavior of the mobility curve for $T > 100$ K is basically the same as the one in the dark condition. However, for temperatures below 100 K, the carrier mobility becomes smaller than the mobility values in dark conditions. Charge carrier mobility depends on its effective mass and scattering time. Since the theory has indicated that both of these quantities can be strongly dependent on the carrier density in semiconductors, we believe that the increase in the carrier concentration for $T < 100$ K can lead to a decrease in the carrier mobility under light conditions. Such behavior was also observed in the PbTe QW at low temperatures.[21]

The basic processes that govern the magnitude of the photoconductivity are the generation of electrons and holes through the absorption of incident photons and their recombination. In the presence of trap levels, a significant fraction of photogenerated carriers may become immobilized. The photoexcitation may change both the carrier density and the carrier mobility, thus the variation of the electrical conductivity under illumination can be described by a simple classic model as

$$\Delta\sigma = q\mu_0\Delta p + (p_0 + \Delta p)q\Delta\mu, \qquad (1)$$

where q is the electronic charge, p_0 and μ_0 are the carrier density and mobility in the dark, respectively, $\Delta p = p_{light} - p_0$, and $\Delta\mu = \mu_{light} - \mu_0$. This model predicts that the NPC effect can be observed in the case of $\Delta p < 0$ and/or $\Delta\mu < 0$.

Figure 4(c) shows $\Delta\sigma$ obtained from Fig. 2(b) (open circles) together with $\Delta\sigma$ calculated from Eq. (1) (solid line) using the Hall data. According to this figure, the experimental values are close to the ones calculated from Eq. (1) for temperatures above 4.2 K. Hence, the model predicts a transition from positive to negative photoconductivity at

Published under an exclusive license by AIP Publishing

4.2 K by taking into account the carrier density and mobility variations. In this case, the model shows that the NPC is mainly caused but a reduction of carrier mobility under illumination ($\Delta\mu < 0$). However, the $\Delta\sigma$ amplitude calculated by the theoretical model deviates from the experimental values for the temperature range of $T = 3.5$–1.9 K. The same deviation between theoretical and experimental values is observed when the sample is under IR illumination, see Fig. 4(d). The origin of this discrepancy at lower temperatures indicates that Eq. (1) does not take all effects present in this temperature region.

We have also investigated the magnetic field (B) dependence of the photoconductivity to verify its influence on the NPC effect observed in the SnTe quantum well under UV light. Figure 5(a) shows the longitudinal resistance (R_{xx}) as a function of the magnetic field B applied perpendicularly to the sample surface under dark and light conditions at 3 K. At a low magnetic field, the dark resistance presents a sharp increase in R_{xx} that characterizes the presence of the weak antilocalization (WAL) effect. We also verify the possible contribution from topological surface states to the NPC effect investigating the presence of quantum oscillations.[17] The presence of quantum oscillations can be verified if the second derivative of the longitudinal resistance with respect to the magnetic field is applied. The inset in Fig. 5(a) shows the curve of d^2R_{xx}/dB^2 as a function of B at 3 K, where there is no presence of beating patterns. The absence of oscillations in the magnetoresistance curves indicates that the topological surface states do not contribute to the NPC effect. Moreover, a transition from negative to positive photoconductivity has also been observed at 0.7 T, and it can be better observed in Fig. 5(b) (indicated by the arrow). These results reveal that the NPC effect can be easily suppressed by the magnetic field, which can be interesting from the viewpoint of applications in devices. This interesting behavior of suppression of negative photoconductivity by the magnetic field may be correlated with the electron mobility, which influences the recombination rates of the carriers.

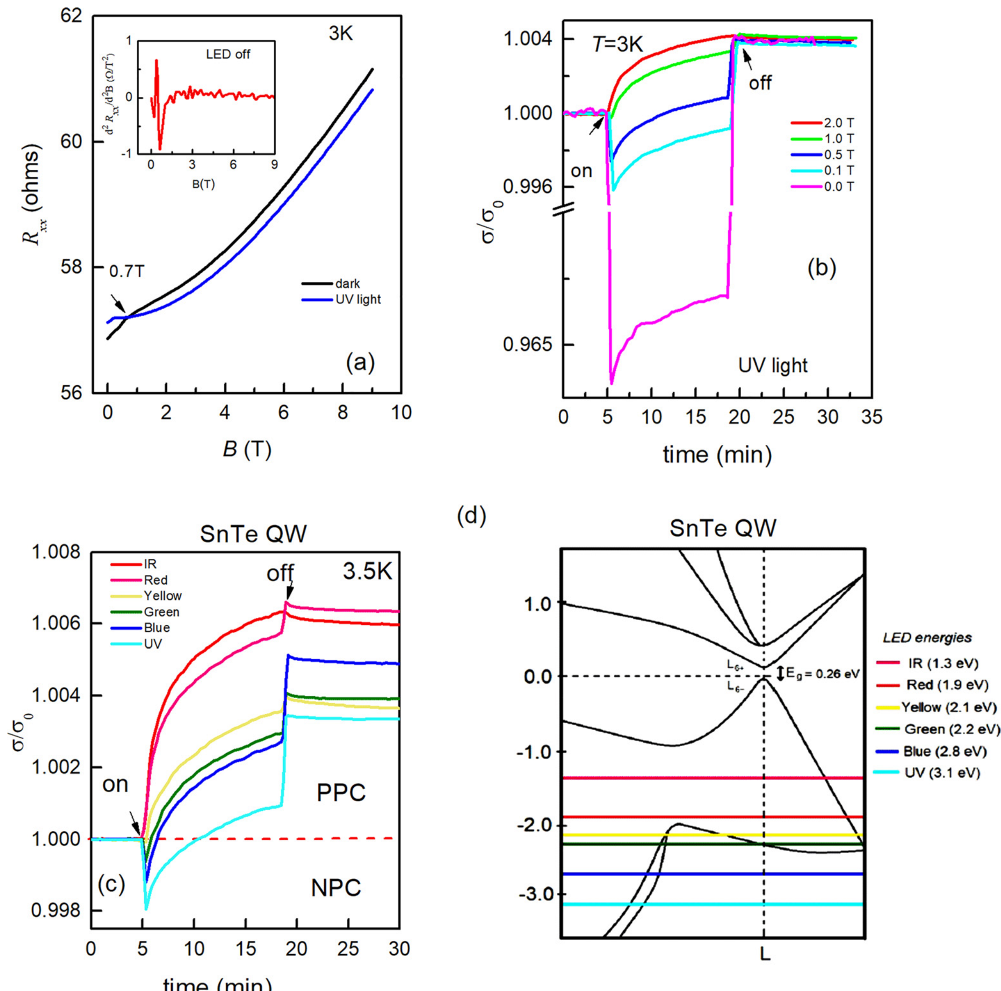

FIG. 5. (a) Longitudinal resistance (R_{xx}) as a function of the magnetic field applied perpendicularly to the *p*-type SnTe QW sample surface. The inset shows the curve of d^2R_{xx}/dB^2 as a function of B at 3 K, where there is no presence of beating patterns. In this figure, it is clear the presence of WAL. (b) Time dependence of the normalized photoconductivity under different magnetic fields at 3 K. We can see that the magnetic field influences the amplitude of the NPC effect. (c) Evolution of the photoconductivity with different wavelengths of incident light for sample A2 at 3.5 K. (d) Pictorial representation of the band structure of SnTe. The horizontal lines represent the energy of the LEDs.

Published under an exclusive license by AIP Publishing

It has been reported that in systems with magnetic or ionized impurities, an increase in the mobility upon magnetic field can be associated with the decrease in the spin-flip scattering.[22,23] Since the recombination rate should decrease with increasing mobility, it is expected a reduction of the NPC effect with the increase in the magnetic field. Such behavior is clearly observed in Fig. 5(b), where a transition from NPC to PPC occurs when the magnetic field increases from 0 to 2.0 T.

Despite the change in carrier concentration being the origin of the photoconductivity effect observed in the SnTe QW, in the present case, our results indicate that a small change in mobility made the major contribution to the negative photoconductivity. Furthermore, since the NPC was observed only when the sample was illuminated by UV light, we believe that the band above 2 eV is also responsible for the effect observed. To investigate both the influence of the band above 2 eV and the mobility in the NPC mechanism, a detailed study of the photoconductivity effect was performed in another SnTe QW (sample A2) that presents slightly higher mobility, μ_2, than sample A1 ($\mu_1 = 51.4$ and $\mu_2 = 56.9\,cm^2/V\,s$). Figure 5(c) illustrate the photoconductivity behavior of sample A2 under LED excitations at 398, 449, 568, 591, 634, and 950 nm at 3.5 K. First, we observe that the positive photoconductivity decreases gradually by reducing the light wavelength from 950 nm (1.3 eV-IR light) to 634 nm (1.9 eV-red light). The positive photoconductivity can be understood by the light-induced electron–holes pairs, which increase the carrier concentration when the light energy increases from IR to red. The increase in the carrier concentration leads to a decrease in the mobility of the carriers, which means changes in the intensity of the photoconductivity. From 591 (yellow LED-2.1 eV) to 398 nm (UV light-3.1 eV), the NPC effect was observed at the beginning of the illumination, and then the effect becomes positive.

In order to illustrate this assumption, Fig. 5(d) presents a schematic representation of the band structure of the SnTe, where the energies' positions according to the LED energies are indicated by the solid lines. This diagram illustrates that when the LED energy approaches to the energies around 2 eV, the NPC manifests itself, which is in accordance with Fig. 5(c).

We have investigated the origin of the NPC effect observed on the *p*-SnTe QW sample. We showed that a strong dependence of the photoconductivity on the incident radiation wavelength is observed and that it is possible to tune the photoconductivity from positive to negative. A systematic analysis of the photoconductivity indicates that the origin of the NPC is not related to the topological surface states, but it is probably due to the dynamic between the carrier mobility and concentration when the sample is under illumination. In addition, the strong persistent effect observed can be explained due to the influence of the trap level in the dynamics of the recombination rates.

The authors thank CAPES for financial support.

DATA AVAILABILITY

The data that support the findings of this study are available from the corresponding author upon reasonable request.

REFERENCES

[1] S. C. Singh, Y. Peng, J. Rutledge, and C. Guo, "Photothermal and Joule-heating-induced negative-photoconductivity-based ultraresponsive and near-zero-biased copper selenide photodetectors," ACS Appl. Electron. Mater. **1**(7), 1169–1178 (2019).
[2] K. Park, M. Jung, D. Kim, J. R. Bayogan, J. H. Lee, S. J. An, J. Seo, J. Seo, J. Ahn, and J. Park, Nano Lett. **20**, 4939 (2020).
[3] J. Cha, J. H. Han, W. Yin, C. Park, Y. Park, T. K. Ahn, J. H. Cho, and D. Jung, J. Phys. Chem. Lett. **8**, 565 (2017).
[4] H. Zhou, L. Cong, J. Ma, B. Li, M. Chen, H. Xu, and Y. Liua, J. Mater. Chem. C **7**, 13149 (2019).
[5] M. G. Burdanova, A. P. Tsapenko, D. A. Satco, R. Kashtiban, C. D. W. Mosley, M. Monti, M. Staniforth, J. Sloan, Y. G. Gladush, A. G. Nasibulin, and J. Lloyd-Hughes, ACS Photonics **6**, 1058 (2019).
[6] M. A. B. Tavares, M. J. da Silva, M. L. Peres, S. de Castro, D. A. W. Soares, A. K. Okazaki, C. I. Fornari, P. H. O. Rappl, and E. Abramof, Appl. Phys. Lett. **110**, 042102 (2017).
[7] M. J. P. Pirralho, M. L. Peres, D. A. W. Soares, P. C. O. Braga, F. S. Pena, C. I. Fornari, P. H. O. Rappl, and E. Abramof, Phys. Rev. B **95**, 075202 (2017).
[8] M. J. P. Pirralho, M. L. Peres, F. S. Pena, R. S. Fonseca, D. da Cruz Alves, D. A. W. Soares, C. I. Fornari, P. H. O. Rappl, and E. Abramof, Mater. Res. Express **6**, 025915 (2018).
[9] S. Gu, K. Ding, J. Pan, Z. Shao, J. Mao, X. Zhanga, and J. Jie, J. Mater. Chem. A **5**, 11171 (2017).
[10] Y. Pei, L. Zheng, W. Li, S. Lin, Z. Chen, Y. Wang, X. Xu, H. Yu, Y. Chen, and B. Ge, Adv. Electron. Mater. **2**, 1600019 (2016).
[11] R. Moshwan, L. Yang, J. Zou, and Z.-G. Chen, "Eco-friendly SnTe thermoelectric materials: Progress and future challenges," Adv. Funct. Mater. **27**(43), 1703278 (2017).
[12] Z. Weng, S. Ma, H. Zhub, Z. Ye, T. Shu, J. Zhouc, X. Wu, and H. Wu, Sol. Energy Mater. Sol. Cells **179**, 276 (2018).
[13] T. Jiang, Y. Zang, H. Sun, X. Zheng, Y. Liu, Y. Gong, L. Fang, X. Cheng, and K. He, Adv. Opt. Mater. **5**, 1600727 (2017).
[14] T. H. Hsieh, H. Lin, J. Liu, W. Duan, A. Bansil, and L. Fu, "Topological crystalline insulators in the SnTe material class," Nat. Commun. **3**, 982 (2013).
[15] B. A. Assaf, F. Katmis, P. Wei, B. Satpati, Z. Zhang, S. P. Bennett, V. G. Harris, J. S. Moodera, and D. Heiman, Appl. Phys. Lett. **105**, 102108 (2014).
[16] S. Safaei, M. Galicka, P. Kacman, and R. Buczko, "Quantum spin Hall effect in IV-VI topological crystalline insulators," New J. Phys. **17**(6), 063041 (2015).
[17] A. K. Okazaki, S. Wiedmann, S. Pezzini, M. L. Peres, P. H. O. Rappl, and E. Abramof, "Shubnikov–de Haas oscillations in topological crystalline insulator SnTe(111) epitaxial films," Phys. Rev. B **98**(19), 195136 (2018).
[18] J. A. H. Coaquira, V. A. Chitta, N. F. Oliveira, Jr., P. H. O. Rappl, A. Y. Ueta, E. Abramof, and G. Bauer, J. Supercond. **16**, 115 (2003).
[19] S. D. Castro, D. A. W. Soares, M. L. Peres, P. H. O. Rappl, and E. Abramof, "Room temperature persistent photoconductivity in p-PbTe and p-PbTE:BaF_2," Appl. Phys. Lett. **105**(16), 162105 (2014).
[20] N. Kumar and A. Srivastava, "Faster photoresponse, enhanced photosensitivity and photoluminescence in nanocrystalline ZnO films suitably doped by Cd," J. Alloys Compd. **706**, 438–446 (2017).
[21] F. S. Pena, M. L. Peres, M. J. P. Pirralho, D. A. W. Soares, C. I. Fornari, P. H. O. Rappl, and E. Abramof, Appl. Phys. Lett. **111**, 192105 (2017).
[22] C. Haas, Phys. Rev. **168**(2), 531 (1968).
[23] P. N. Argyres and E. N. Adams, "Longitudinal magnetoresistance in the quantum limit," Phys. Rev. **104**(4), 900–908 (1956).

Published under an exclusive license by AIP Publishing